

## The CMSSM Parameter Space at Large $\tan\beta$

John Ellis<sup>1</sup>, Toby Falk<sup>2</sup>, Gerardo Ganis<sup>3</sup>, Keith A. Olive<sup>1,2</sup> and Mark Srednicki<sup>4</sup>

<sup>1</sup>*TH Division, CERN, Geneva, Switzerland*

<sup>2</sup>*Theoretical Physics Institute, School of Physics and Astronomy,  
University of Minnesota, Minneapolis, MN 55455, USA*

<sup>3</sup>*INFN, Università di Roma II 'Tor Vergata', Rome, Italy*

<sup>4</sup>*Department of Physics, University of California, Santa Barbara, CA 93106, USA*

### Abstract

We extend previous combinations of LEP and cosmological relic density constraints on the parameter space of the constrained MSSM, with universal input supersymmetry-breaking parameters, to large  $\tan\beta$ . We take account of the possibility that the lightest Higgs boson might weigh about 115 GeV, but also retain the possibility that it might be heavier. We include the most recent implementation of the  $b \rightarrow s\gamma$  constraint at large  $\tan\beta$ . We refine previous relic density calculations at large  $\tan\beta$  by combining a careful treatment of the direct-channel Higgs poles in annihilation of pairs of neutralinos  $\chi$  with a complete treatment of  $\chi - \tilde{\tau}$  coannihilation, and discuss carefully uncertainties associated with the mass of the  $b$  quark. We find that coannihilation and pole annihilations allow the CMSSM to yield an acceptable relic density at large  $\tan\beta$ , but it is consistent with all the constraints only if  $m_\chi > 140$  (180) GeV for  $\mu > 0$  ( $\mu < 0$ ) for our default choices  $m_b(m_b)_{\overline{MS}} = 4.25$  GeV,  $m_t = 175$  GeV, and  $A_0 = 0$ .

Now that LEP has been terminated, and future accelerator constraints on supersymmetry may take a while to accumulate, it is important to extract the last drop of phenomenological information from the completed LEP searches [1, 2]. The constraints from LEP are particularly interesting when combined with the measured value of the  $b \rightarrow s\gamma$  decay rate [3] and with restrictions on cold dark matter imposed by astrophysics and cosmology, assuming that the lightest supersymmetric particle (LSP) is the lightest neutralino  $\chi$  [4], and that  $R$  parity is conserved. We [5, 6, 7, 8] and others [9, 10, 11, 12, 13, 14, 15] have made such combinations, in both the generic minimal supersymmetric extension of the Standard Model (MSSM) and with the supplementary constraint that the soft supersymmetry-breaking scalar masses be universal at some high input scale (CMSSM), as in minimal supergravity (mSUGRA) models [16]. We limited our previous analyses [5, 6, 8] to  $\tan\beta \leq 20$ , because the available  $b \rightarrow s\gamma$  calculations [17] were not applicable to larger values of  $\tan\beta$ , and because we were dissatisfied with the reliability and accuracy of the available calculations at larger  $\tan\beta$  of the relic density  $\Omega_\chi h^2$ , for which we regard  $0.1 \leq \Omega_\chi h^2 \leq 0.3$  as the cosmologically-favoured range.

Concerning the first point, we note that new and improved calculations for large  $\tan\beta$  have recently come available [18], and we implement them in our analysis. Concerning  $\Omega_\chi h^2$ , we note two important issues. The first is that  $\chi - \tilde{\ell}$  coannihilation effects are important in the CMSSM [6], and the second is that direct-channel annihilations through poles [19] due to the heavier neutral MSSM Higgs bosons  $H$  and  $A$  are of increasing importance for larger  $\tan\beta$  [10, 11, 20].

We recall that, in the CMSSM, the next-to-lightest supersymmetric particle (NLSP) is the lighter stau  $\tilde{\tau}_1$  in a generic domain of parameter space, and  $\chi - \tilde{\tau}, \tilde{\mu}$  and  $\tilde{e}$  coannihilations are important for calculating the relic density<sup>1</sup>. The most complete published  $\chi - \tilde{\ell}$  coannihilation calculations known to us are those in [6, 14], but more  $\chi - \tilde{\tau}$  coannihilation diagrams become potentially relevant at large  $\tan\beta$ .

As for the  $A, H$  poles, we recall that, unlike the lightest MSSM Higgs boson  $h$ , the masses and total decay widths of the  $H$  and  $A$  increase with the soft supersymmetry-breaking parameters  $m_0, m_{1/2}$ , enhancing their significance. An accurate treatment of the bottom-quark mass  $m_b$ , its renormalization and that of the corresponding Yukawa coupling is important for the correct calculation of the Higgs spectrum and couplings at large  $\tan\beta$ . Here we include with similar accuracy the corresponding effects associated with the mass and Yukawa coupling of the  $\tau$  lepton. Calculations of  $\chi - \chi$  annihilations via a series expansion in  $x_f$ , the freeze-out temperature  $T_f$  divided by  $m_\chi$ , are inadequate when  $m_{H,A} \sim 2m_\chi$  and the

---

<sup>1</sup>In the CMSSM, neither  $\chi - \chi' - \chi^\pm$  [21, 12] nor  $\chi - \tilde{t}$  [22] coannihilations are important.

$H$  and  $A$  poles are important. Calculations of  $\chi - \chi$  annihilations that go beyond the  $x_f$  series expansion are available [11, 23], but they have not yet been combined with complete coannihilation calculations at large  $\tan\beta$ . As we see later, there is an important interplay between annihilations via the direct-channel  $A, H$  poles and coannihilation processes.

We find that the CMSSM survives all the experimental and cosmological constraints at large  $\tan\beta$  only thanks to the coannihilation and  $A, H$  pole annihilation effects. Combining the available constraints, we find that  $m_\chi \gtrsim 140$  (180) GeV for  $\mu > 0$  ( $\mu < 0$ ) and our default choices  $m_t = 175$  GeV,  $m_b(m_b)_{\overline{MS}}^{SM} = 4.25$  GeV, and  $A_0 = 0$ . We also find an upper bound  $m_\chi \lesssim 400$  to 550 GeV for  $\tan\beta \geq 20$ , if  $m_h \sim 115$  GeV, as suggested by LEP [2].

The most important experimental constraints on the CMSSM parameter space are provided by LEP searches for sparticles and Higgs bosons [1], the latter constraining the sparticle spectrum indirectly via radiative corrections. The kinematic reach for charginos was  $m_{\chi^\pm} = 104$  GeV, and the LEP limit is generally close to this value, within the CMSSM framework. The LEP searches for sleptons impose  $m_{\tilde{e}} > 97$  GeV,  $m_{\tilde{\mu}} > 94$  GeV and  $m_{\tilde{\tau}} > 80$  GeV for  $m_\chi < 80$  GeV. The only one of these to fall noticeably below the limit expected statistically is that on the  $\tilde{\tau}$ , but this is not interpreted as significant evidence for a  $\tilde{\tau}$ . Other important sparticle constraints are those on stop squarks  $\tilde{t}$ :  $m_{\tilde{t}} > 94$  GeV for  $m_\chi < 80$  GeV from LEP, and  $m_{\tilde{t}} \gtrsim 115$  GeV for  $m_\chi \lesssim 50$  GeV from the Fermilab Tevatron collider [24].

The lower limit on the mass of a Standard Model Higgs boson imposed by the combined LEP experiments is 113.5 GeV [2]. This lower limit applies also to the MSSM for small  $\tan\beta$ , even if squark mixing is maximal. In the CMSSM, maximal mixing is not attained, and the  $e^+e^- \rightarrow Z^0 + h$  production rate is very similar to that in the Standard Model [25], for all values of  $\tan\beta$ . As is well known, a 2.9- $\sigma$  signal for a Higgs boson weighing about  $115_{-0.7}^{+1.3}$  GeV has been reported [2]. At points in the following, we comment explicitly on the possible implications if  $m_h \sim 115$  GeV [8]. In order to account for uncertainties in theoretical calculations of  $m_h$  in the MSSM [26] for any given value of  $m_t$ , we consider this LEP range [2] to be consistent with CMSSM parameter choices that yield  $113 \text{ GeV} \leq m_h \leq 117 \text{ GeV}$ . The theoretical value of  $m_h$  in the MSSM is quite sensitive to  $m_t$ , the pole mass of the top quark: we use  $m_t = 175$  GeV as default, but also discuss briefly the cases  $m_t = 170, 180$  GeV.

We implement the new NLO  $b \rightarrow s\gamma$  calculations of [18] when  $\tilde{M} > 500$  GeV, where  $\tilde{M} = \text{Min}(m_{\tilde{q}}, m_{\tilde{g}})$ . Otherwise, we use only the LO calculations and assign a larger theoretical error. For the experimental value, we combine the CLEO measurement with the recent BELLE result [3], assuming full correlation between the experimental systematics <sup>2</sup>, finding

---

<sup>2</sup>This is conservative, but the available information does not justify a more restrictive approach, and this assumption is in any case not very important.

$\mathcal{B}(b \rightarrow s\gamma) = (3.21 \pm 0.44 \pm 0.26) \times 10^{-4}$ . In our implementation, we allow CMSSM parameter choices that, after including the theoretical errors due to the scale and model dependences, may fall within the 95% confidence level range  $2.33 \times 10^{-4} < \mathcal{B}(b \rightarrow s < \gamma) < 4.15 \times 10^{-4}$ . In general, we find in the regions excluded when  $\mu < 0$  that the predicted value of  $\mathcal{B}(b \rightarrow s\gamma)$  is larger than this measured range, whereas, when  $\mu > 0$ , the exclusion results from  $\mathcal{B}(b \rightarrow s\gamma)$  being smaller than measured.

There is a tendency for the masses of the (nearly degenerate)  $H$  and  $A$  bosons to drop at large  $\tan\beta$  in the CMSSM, and hence for strong direct-channel annihilation:  $\chi\chi \rightarrow H, A \rightarrow X$  become possible when  $m_{H,A} \sim 2m_\chi$ . Annihilation via the  $A$  pole to  $\bar{b}b$  is additionally enhanced because of the large  $A\bar{b}b$  coupling at large  $\tan\beta$ . The  $H\bar{b}b$  coupling is equally enhanced, but the  $A$  pole is more important because direct-channel pseudoscalar exchange to  $\bar{f}f$  final states is not  $P$ -wave suppressed. In view of the importance of the direct-channel  $A$  pole at large  $\tan\beta$ , we take pains to include the most accurate available calculation of  $m_A$ , which incorporates a renormalization-group (RG) improvement of the standard effective potential calculation, so as to take into account the leading effects associated with the third-generation Yukawa couplings<sup>3</sup>. This calculation may be extracted from [28], setting to zero the CP-violating phases. We parametrize the tree-level MSSM Higgs potential in the usual way, denoting by  $m_{12}^2$  the coefficient of the  $H_1^\dagger H_2$  term in the effective lagrangian, and include one-loop corrections due to the  $\tau$  lepton and the  $\tilde{\tau}$  sleptons and the  $b$  supermultiplet - in view of their potential importance at large  $\tan\beta$  - as well as the  $t$  supermultiplet. The RG-improved pseudoscalar MSSM Higgs mass is then given by

$$m_A^2 = \frac{\text{Rem}_{12}^2 + \text{Rem}_{12}^{2(1)}}{\sin\beta \cos\beta} + \sum_{f=t,b,\tau} \frac{(\Delta\mathcal{M}_A^2)^{\bar{f}}}{\xi_1^{\bar{f}}(m_t)\xi_2^{\bar{f}}(m_t)} \quad (1)$$

where  $\text{Rem}_{12}^{2(1)}$  is taken from equation (3.7) of [28],  $(\Delta\mathcal{M}_A^2)^{\bar{f}}$  is the standard one-loop contribution to  $m_A^2$  due to the third-generation fermions  $f$ , and  $\xi_{1(2)}^{\bar{f}}(m_t)$  are anomalous-dimension factors taken from equation (3.25) of [28]<sup>4</sup>.

It is well known that the partial-wave expansion breaks down in the vicinity of poles [19], whose finite widths must be taken into account. We calculate these including all the SM final states and relevant QCD corrections [29]. To account for the poles, we perform the full phase-space integration [11] for the direct-s channel  $A$  and  $H$  exchanges in the vicinities of

---

<sup>3</sup>It might also be desirable to include the corresponding improvement linked to gauge couplings [27], but we do not have these available, and they are likely to be less important.

<sup>4</sup>On the other hand, we do not include the corresponding RG improvements to  $m_{h,H,H^\pm}$  [28], which are more complicated but less essential for our purposes. The effects of the direct-channel  $H$  pole are hidden by the more important effects of the almost degenerate  $A$  pole.

their poles, namely for  $0.65 < 2m_\chi/m_{A,H} < 2.0$ . This full phase-space integration must be performed for temperatures  $T$  down to the freeze-out temperature  $T_f = x_f \times m_\chi$ . When the direct-channel poles are important, we determine the correct freeze-out temperature iteratively.

As already mentioned,  $\chi - \tilde{\ell}$  coannihilation - particularly that with the lighter stau  $\tilde{\tau}_1$  - is important in the CMSSM, extending significantly the allowed range of  $m_{1/2}$ . The most complete available calculations of  $\chi - \tilde{\ell}$  coannihilation [6] are, however, inadequate at large  $\tan\beta$ , for example because the larger  $\tau$  Yukawa coupling in this limit increases the importance of diagrams that were negligible for smaller  $\tan\beta$ . In updating our coannihilation code, we have also taken the opportunity to complete and improve some of its other aspects. The following are the most important modifications: (a)  $\tilde{\tau}_1 - \tilde{\tau}_2$  mixing has been incorporated fully (previously, it was incorporated in the kinematics but not in the couplings), (b)  $m_\tau$  effects have been included in  $\tilde{\tau} - \tilde{e}, \tilde{\mu}$  coannihilations, (c) crossed-channel  $\tilde{\tau}_2$ -exchange diagrams have been included for coannihilations into the following final states:  $Z^0 Z^0, Z^0 h, hh, \tau Z^0, \tau h$ , and (d) sub-routines for the following final states:  $Z^0 H, \gamma H, hA, HA, W^\pm H^\mp, AA, hH, HH, H^+ H^-, \tau H$  and  $\tau A$  have been included in the code used to obtain the results we present here <sup>5</sup>. Results for some of these processes were previously presented in [6], but they were kinematically inaccessible in the region of interest there. We find that for  $\tan\beta \leq 20$  inclusion of the new coannihilation effects does not alter significantly the region of the  $(m_{1/2}, m_0)$  plane favoured by cosmology, whereas for  $\tan\beta \geq 30$  there is a significant increase of the favoured range of  $m_{1/2}$  in the coannihilation region, as we discuss in more detail later.

Since the precise value of the  $b$ -quark mass  $m_b$  is important at large  $\tan\beta$ , we now discuss it in some detail. Various different definitions of  $m_b$  have been proposed, and we prefer the running mass in the  $\overline{MS}$  renormalization prescription for the Standard Model (SM):  $m_b(m_b)_{\overline{SM}}^{\overline{MS}}$ . A recent determination of  $m_b(m_b)_{\overline{SM}}^{\overline{MS}}$  from a combination of lattice calculations and experimental measurements of the masses of  $B$  mesons [31] yields  $m_b(m_b)_{\overline{SM}}^{\overline{MS}} = 4.25 \pm 0.15$  GeV <sup>6</sup>. We therefore take as our default value  $m_b(m_b)_{\overline{SM}}^{\overline{MS}} = 4.25$  GeV, but also discuss later the change in physics if  $m_b(m_b)_{\overline{SM}}^{\overline{MS}} = 4.0$  or  $4.5$  GeV, regarding this as a full  $\pm 2 - \sigma$  range. We note that this is similar to the range quoted by the Particle Data Group [32]. Having fixed the input value, we then evolve the running mass  $m_b(Q)_{\overline{SM}}^{\overline{MS}}$  from  $Q = m_b$  up to  $Q = m_Z$  using the three-loop  $\overline{MS}$  RGE's for the Standard Model [34]

$$m_b(m_Z)_{\overline{SM}}^{\overline{MS}} = m_b(m_b)_{\overline{SM}}^{\overline{MS}} \left[ \frac{\alpha_s(m_Z)}{\alpha_s(m_b)} \right]^{12/23} \frac{c[\alpha_s(m_Z)/\pi]}{c[\alpha_s(m_b)/\pi]} \quad (2)$$

<sup>5</sup>Details of these calculations will appear in [30].

<sup>6</sup>This also includes the ranges favoured by recent sum-rule analyses of  $\Upsilon$  masses [33].

where

$$c[\alpha_s] = 1 + 1.175\alpha_s + 1.501\alpha_s^2 - 0.172\alpha_s^3 \quad (3)$$

which we evaluate using  $\alpha_s(4.25 \text{ GeV}) = 0.2246$  and  $\alpha_s(m_Z) = 0.1185$ . We then convert  $m_b$  to the  $\overline{DR}$  scheme, using the one-loop correction factor

$$m_b(m_Z)_{\overline{DR}}^{SM} = m_b(m_Z)_{\overline{MS}}^{SM} \times [1 - (\alpha_s/3\pi) + (3\alpha_2/32\pi)] \quad (4)$$

valid in the Standard Model [35]. We then make the further correction to convert from the Standard Model value  $m_b(m_Z)_{\overline{DR}}^{SM}$  to the MSSM value  $m_b(m_Z)_{\overline{DR}}^{MSSM}$  [36]. Finally, we use the MSSM  $\overline{DR}$  RGE's at scales between  $m_Z$  and the unification scale [37]. We use the running  $m_{b,t}(Q = 2m_\chi)$  when evaluating annihilation processes.

Since it is of interest for most sparticle searches, and for ease of comparison with our previous results, we first present results in the  $(m_{1/2}, m_0)$  plane. For definiteness, as default we choose the trilinear soft supersymmetry-breaking parameter  $A_0 = 0$  at the input GUT scale, and determine  $\mu$  (up to a sign ambiguity) from the electroweak vacuum conditions for the specified value of  $\tan\beta$ . We also use as default  $m_t = 175 \text{ GeV}$  for the on-shell top-quark mass. With our default choices, and if  $\mu < 0$ , there are no large regions with consistent electroweak vacua for  $\tan\beta \geq 40$ , and we do not expect our new results to differ significantly from our previous results [6] for  $\tan\beta < 20$ . We display in Fig. 1 the  $(m_{1/2}, m_0)$  planes for  $\mu < 0$  and  $\tan\beta = 20, 30, 35$  and  $37.5$ . We see that the LEP Higgs constraint and  $b \rightarrow s\gamma$  each exclude large regions with small  $m_{1/2}$ : the only supersymmetric dark matter regions to survive for  $\mu < 0$  are those made possible by  $\chi - \tilde{\ell}$  coannihilation and/or rapid annihilations via the  $A, H$  poles.

We see in panel (a) that our new results are indeed very similar to our previous results [6] for  $\tan\beta = 20$ . The only (small) differences are due to the improved treatment of  $m_b$  discussed above, which is relevant in the region  $m_0 \sim m_{1/2} \sim 200 \text{ GeV}$ , and at the boundary of the coannihilation region. On the other hand, we see a dramatic new feature in panels (b), (c) and (d) of Fig. 1 for  $\tan\beta \geq 30$ : rapid annihilation through the direct-channel  $A, H$  poles suppresses the relic density:  $\Omega_\chi h^2 < 0.1$  along a steep diagonal strip in the  $(m_{1/2}, m_0)$  plane where  $m_\chi \sim m_A/2$ . This is flanked by two allowed bands where  $0.1 < \Omega_\chi h^2 < 0.3$ , that connect with the  $\chi - \tilde{\tau}$  coannihilation region on one side and with the low- $m_{1/2}$  region on the other side. This feature develops first at a relatively large ratio of  $m_{1/2}/m_0$  for  $\tan\beta = 30$ , and that the ratio decreases as  $\tan\beta$  increases <sup>7</sup>. Although difficult to see, there

---

<sup>7</sup>Conversely, for smaller values of  $\tan\beta$ , the  $A, H$ -annihilation strip appears at larger  $m_{1/2}$ , not intersecting the cosmologically-preferred region identified previously [6], and the direct-channel  $A, H$  pole is not important.

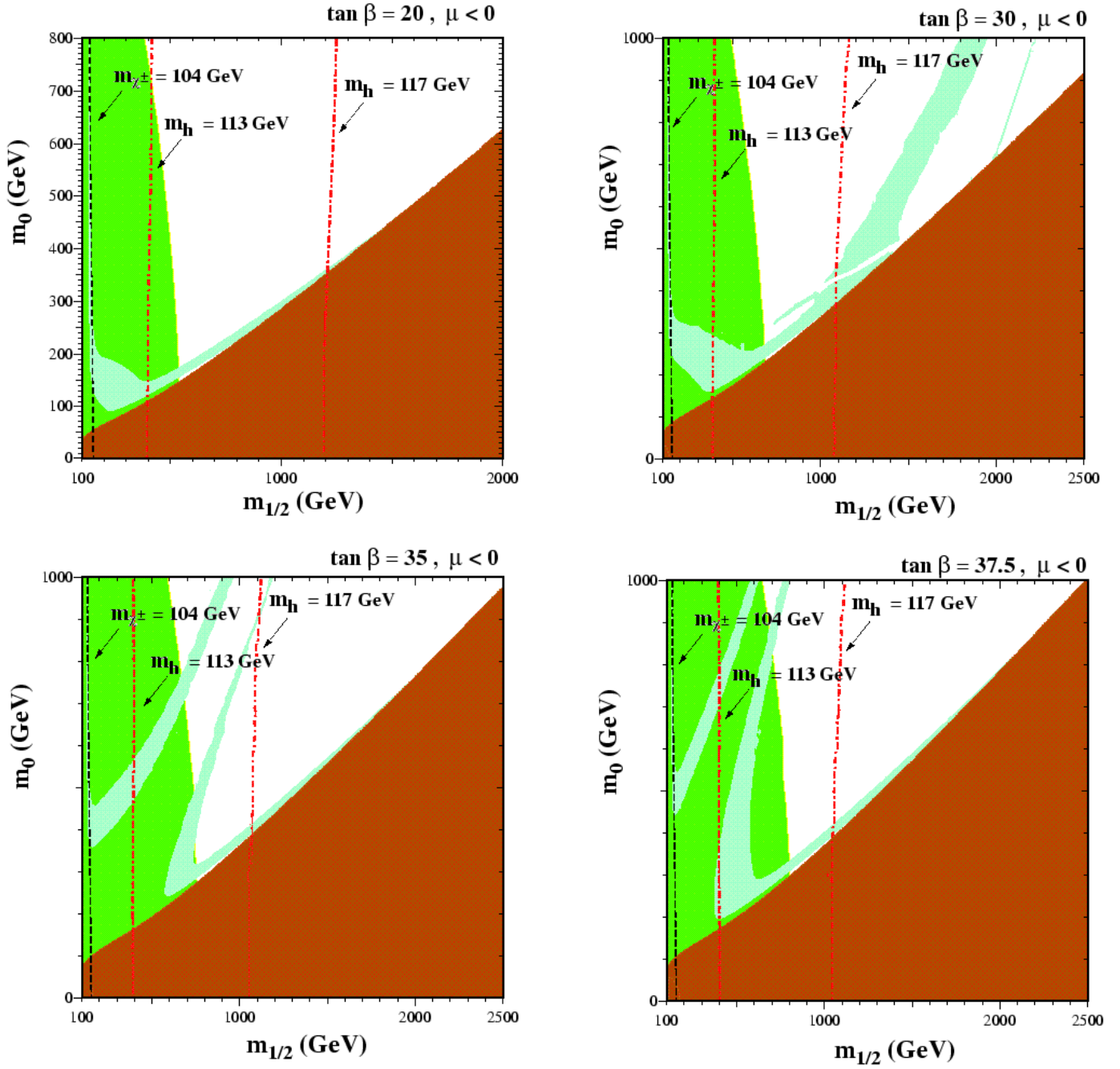


Figure 1: The  $(m_{1/2}, m_0)$  planes for  $\mu < 0$  and  $\tan \beta = (a) 20, (b) 30, (c) 35$  and  $(d) 37.5$ , found assuming  $A_0 = 0, m_t = 175$  GeV and  $m_b(m_b)_{\overline{MS}}^{SM} = 4.25$  GeV. In this case, we find no large allowed region for  $\tan \beta \geq 40$ . The near-vertical are the contours  $m_{\chi_{\pm}} = 104$  GeV (dashed),  $m_h = 113, 117$  GeV (dot-dashed). The medium (dark green) shaded regions are excluded by  $b \rightarrow s\gamma$ . The light (turquoise) shaded areas are the cosmologically preferred regions with  $0.1 \leq \Omega_{\chi} h^2 \leq 0.3$ . Away from the pole, above (below) these light-shaded areas, the relic density  $\Omega_{\chi} h^2 > 0.3 (< 0.1)$ . In the dark (brick red) shaded regions, the LSP is the charged  $\tilde{\tau}_1$ , so this region is excluded. The diagonal channel of low relic densities visible for  $\tan \beta \geq 30$ , flanked on both sides by cosmologically preferred regions, is due to direct-channel annihilation via the  $A, H$  poles.

is a very narrow allowed band to the right of the  $A, H$ -annihilation strip in panel (b) for  $\tan\beta = 30$  with width  $\delta m_{1/2} \sim 15$  GeV, whereas the corresponding band to the left of the  $A, H$ -annihilation strip is clearly visible, with a larger width  $\delta m_{1/2} \sim 150$  GeV. The width of the coannihilation strip that appears when  $m_{\tilde{\tau}_1} \gtrsim m_\chi$  has a width  $\delta m_0 \sim 30$  GeV, which does not depend much on  $\tan\beta$ . However, as seen in panels (c) and (d), the relative widths of the allowed bands on either side of the  $A, H$ -annihilation strip change as  $\tan\beta$  increases<sup>8</sup>.

We also notice in panel (b) another narrow near-horizontal band of suppressed relic density, which meets the first when  $m_{1/2} \sim 1500$  GeV and  $m_0 \sim 500$  GeV, and is due to rapid  $\tilde{\tau}_1 \bar{\tilde{\tau}}_1 \rightarrow H$  annihilation. This not only suppresses the relic density:  $\Omega_\chi h^2 < 0.1$  in a band crossing the left flank of the  $\chi\chi \rightarrow A, H$  annihilation strip, but also suppresses the relic density along a narrow band at lower  $m_{1/2}$ , reducing  $\Omega_\chi h^2$  into the allowed range.

We display in Fig. 2 the corresponding  $(m_{1/2}, m_0)$  planes for  $\mu > 0$  and  $\tan\beta = 30, 40, 50$  and 55. At these large values of  $\tan\beta$ , the constraint on  $m_{1/2}$  from  $m_h$  hardly varies as  $\tan\beta$  increases, and the region excluded by  $b \rightarrow s\gamma$  is much smaller than for  $\mu < 0$ . We also note that there is a small region not excluded by  $b \rightarrow s\gamma$  for  $\mu > 0, m_{1/2} \sim 100$  GeV and  $m_0 \lesssim 300$  GeV, where the conditions for the NLO treatment are not met, so that the theoretical errors are large. However, this region is excluded by the LEP constraint on  $m_h$ .

The principal novelty in panel (a) is that the new coannihilation diagrams and improved treatment of  $\tilde{\tau}$  mixing at large  $\tan\beta$  increase significantly the upper limit on  $m_{1/2}$ . Whereas we previously found [6]  $m_{1/2} \lesssim 1400$  GeV when  $\tan\beta \leq 20$ , as also seen in panel (a) of Fig. 1, we now see that  $m_{1/2} \lesssim 1700$  GeV is allowed for  $\tan\beta = 30$ . Also,  $m_{1/2} \lesssim 1900$  GeV is allowed for  $\tan\beta = 35$ , as seen in panel (c) of Fig. 1, and even larger values of  $m_{1/2}$  are allowed for larger values of  $\tan\beta$  for  $\mu > 0$ , where we find  $m_{1/2} \lesssim 2200$  GeV for  $\tan\beta \sim 50$  as seen in (c, d) of Fig. 2. One effect of this extension of the cosmologically-favoured region to larger  $m_{1/2}$  is that the detection of CMSSM sparticles at the LHC is *not guaranteed* for large  $\tan\beta$ , unlike the case when  $\tan\beta \leq 20$ . At larger  $m_0$ , this extension meets up with the focus point region of [38]. We also see in the panels (b, c) and (d) of Fig. 2 for  $\mu > 0$  the appearance of rapid direct-channel annihilation via the  $A, H$  poles for  $\tan\beta \geq 40$ . We note that this feature develops at larger  $\tan\beta$  than in the case  $\mu < 0$ , and recall that consistent electroweak vacua may readily be found for larger values of  $\tan\beta$ , up to about 60. Detection of CMSSM sparticles at the LHC is *also not guaranteed* in the direct-channel  $A, H$  annihilation region, whose full extent out to large  $m_{1/2}$  and  $m_0$  is not shown: it meets the focus-point regions at

---

<sup>8</sup>We do not discuss here in detail the ‘focus point’ region where an acceptable relic density may be obtained in a band of thickness  $\delta m_0 \sim 30$  GeV when  $m_0 \sim 3$  TeV [38]. We note that our results on  $A, H$  pole effects at large  $\tan\beta$  differ from [38], apparently because of a different treatment of  $m_b$ , in particular.



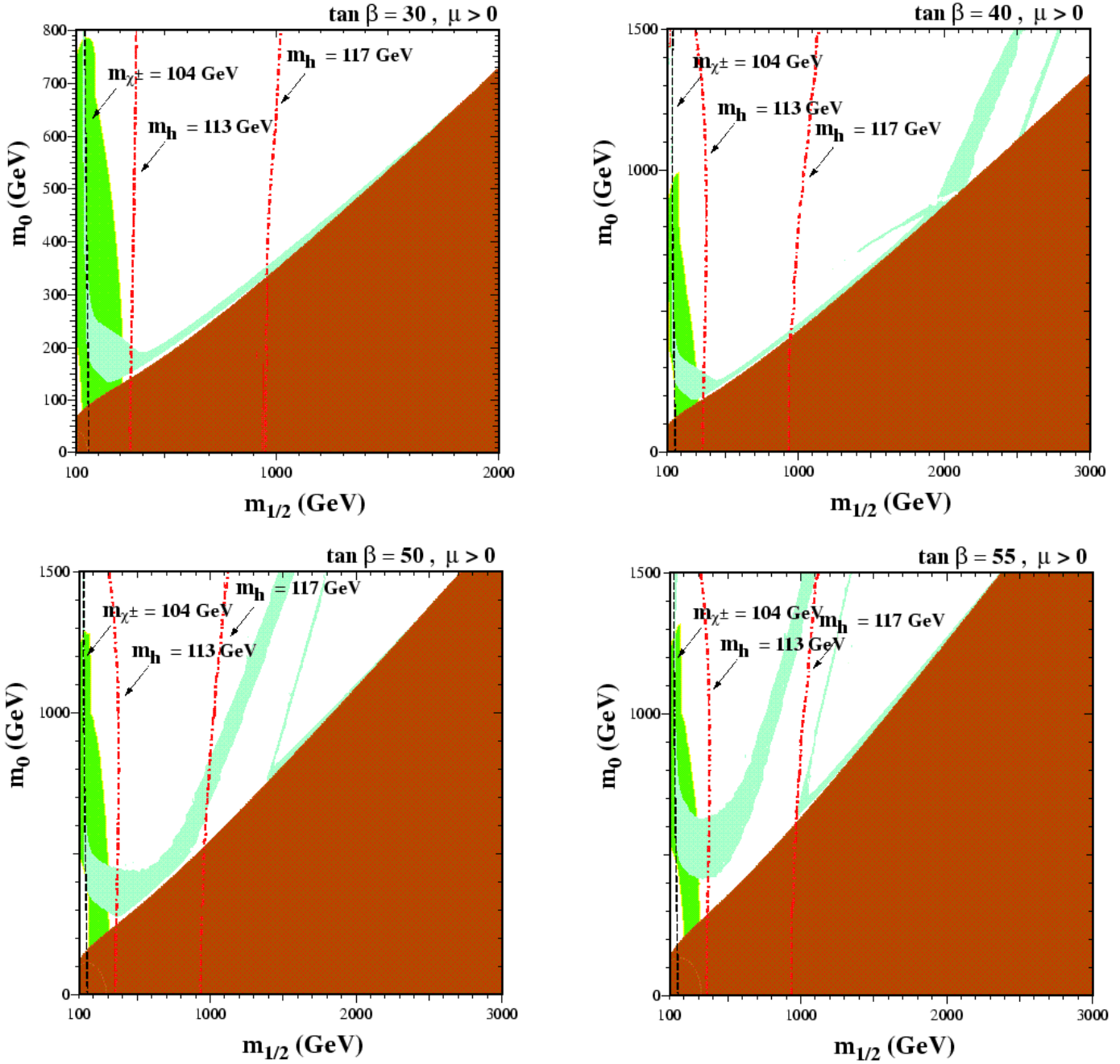


Figure 2: The  $(m_{1/2}, m_0)$  planes for  $\mu > 0$  and  $\tan \beta =$  (a) 30, (b) 40, (c) 50 and (d) 55, found assuming  $A_0 = 0, m_t = 175$  GeV and  $m_b(m_b)_{\overline{MS}} = 4.25$  GeV. The near-vertical lines are the contours  $m_{\chi^\pm} = 104$  GeV (dashed),  $m_h = 113, 117$  GeV (dot-dashed). The medium (dark green) shaded regions are excluded by  $b \rightarrow s\gamma$ . The light (turquoise) shaded areas are the cosmologically preferred regions with  $0.1 \leq \Omega_\chi h^2 \leq 0.3$ . In the dark (brick red) shaded regions, the LSP is the charged  $\tilde{\tau}_1$ , so this region is excluded. The diagonal channel of low relic densities visible for  $\tan \beta \geq 40$ , flanked on both sides by cosmologically preferred regions, is due to direct-channel annihilation via the  $A, H$  poles.

very large  $m_0$ . This LHC-unfriendly  $A, H$  annihilation region is rather larger than the tail of the coannihilation strip at large  $m_{1/2}$ .

The sensitivity to  $m_b(m_b)_{SM}^{\overline{MS}}$  at large  $\tan\beta$  is shown in Fig. 3. Panels (a, b) are for  $\tan\beta = 35$  and  $\mu < 0$ , and panels (c, d) are for  $\tan\beta = 50$  and  $\mu > 0$ . The effect on the LEP Higgs constraint is not important, but the  $b \rightarrow s\gamma$  constraint does depend significantly on  $m_b(m_b)_{SM}^{\overline{MS}}$ . We also see in Fig. 3 that the channel of low relic density due to rapid annihilation via the  $A, H$  poles appears at smaller values of  $m_{1/2}/m_0$  when  $m_b(m_b)_{SM}^{\overline{MS}}$  is larger, because  $m_A$  decreases as  $m_b(m_b)_{SM}^{\overline{MS}}$  increases. The shift in  $m_A$  is quite significant. Consider, for example, the point  $(m_{1/2}, m_0) = (900, 1000)$  for  $\tan\beta = 35$  and  $\mu < 0$ , which is along the cosmologically preferred  $H, A$ -annihilation strip as seen in Fig. 1(c). For  $m_b(m_b)_{SM}^{\overline{MS}} = 4.0, 4.25,$  and  $4.5$  GeV, we find that  $m_A = 1000, 890,$  and  $750$  GeV respectively, whereas, in each case,  $m_\chi = 404$  GeV and  $m_h = 116.3$  GeV. Furthermore, we recall that we did not find consistent electroweak vacua when  $\mu < 0$  and  $\tan\beta \geq 40$  for  $m_b(m_b)_{SM}^{\overline{MS}} = 4.25$  GeV, but, if we choose  $m_b(m_b)_{SM}^{\overline{MS}} = 4.0$  GeV, we find consistent vacuum solutions for  $\mu < 0$  and  $\tan\beta = 40$ . The corresponding  $(m_{1/2}, m_0)$  plane looks qualitatively similar to that in panel (d) of Fig. 1 for  $\mu < 0$  and  $\tan\beta = 37.5$ . This exemplifies the point that, although the appearance of rapid direct-channel  $A, H$ -pole annihilation is a generic qualitative feature at large  $\tan\beta$ , its exact location is rather model- and parameter-dependent.

We have also explored the sensitivity of our analysis to the assumed values of  $m_t$  and  $A_0$ . The  $m_h$  constraint on  $m_{1/2}$  weakens (strengthens) significantly if  $m_t = 180(170)$  GeV [8]. There are smaller effects on the locations of the  $A, H$  poles and hence on the rapid-annihilation regions when  $\mu < 0$ . For positive  $\mu$ , the effects are not negligible, and for  $m_t = 170$  GeV we find that the  $A, H$  annihilation strip is shifted down to lower  $m_{1/2}/m_0$ . If  $A_0$  is varied, again the most significant change is that in the LEP Higgs constraint on  $m_h$ : positive (negative) values of  $A_0$  increase (decrease) the Higgs mass and weaken (strengthen) the limit, whereas changes in  $A_0$  cause only modest changes in the relic density regions. We note also that  $b \rightarrow s\gamma$  is affected slightly by  $m_t$  and to a larger extent by  $A_0$ . We defer detailed discussions of the sensitivity to  $m_t$  and  $A_0$  to a future publication [30].

Finally, we compile our results in Fig. 4 as lower limits on the LSP mass  $m_\chi$  for both signs of  $\mu$  as functions of  $\tan\beta$ , for our default choices  $m_b(m_b)_{SM}^{\overline{MS}} = 4.25$  GeV,  $m_t = 175$  GeV and  $A_0 = 0$ . The curve for  $\mu > 0$  is almost the same as in [8] for  $\tan\beta \leq 25$ . The limits are slightly stronger here, due to the improved treatments of the bottom quark and pseudoscalar mass. The curve for  $\mu < 0$  resembles that in [8] for  $\tan\beta \lesssim 15$ , but deviates at larger  $\tan\beta$  because here we implement the latest  $b \rightarrow s\gamma$  constraint [18]. The monotonic rise in the lower limit on  $m_\chi$  for  $15 \lesssim \tan\beta \lesssim 30$  is due to the strengthening of this constraint

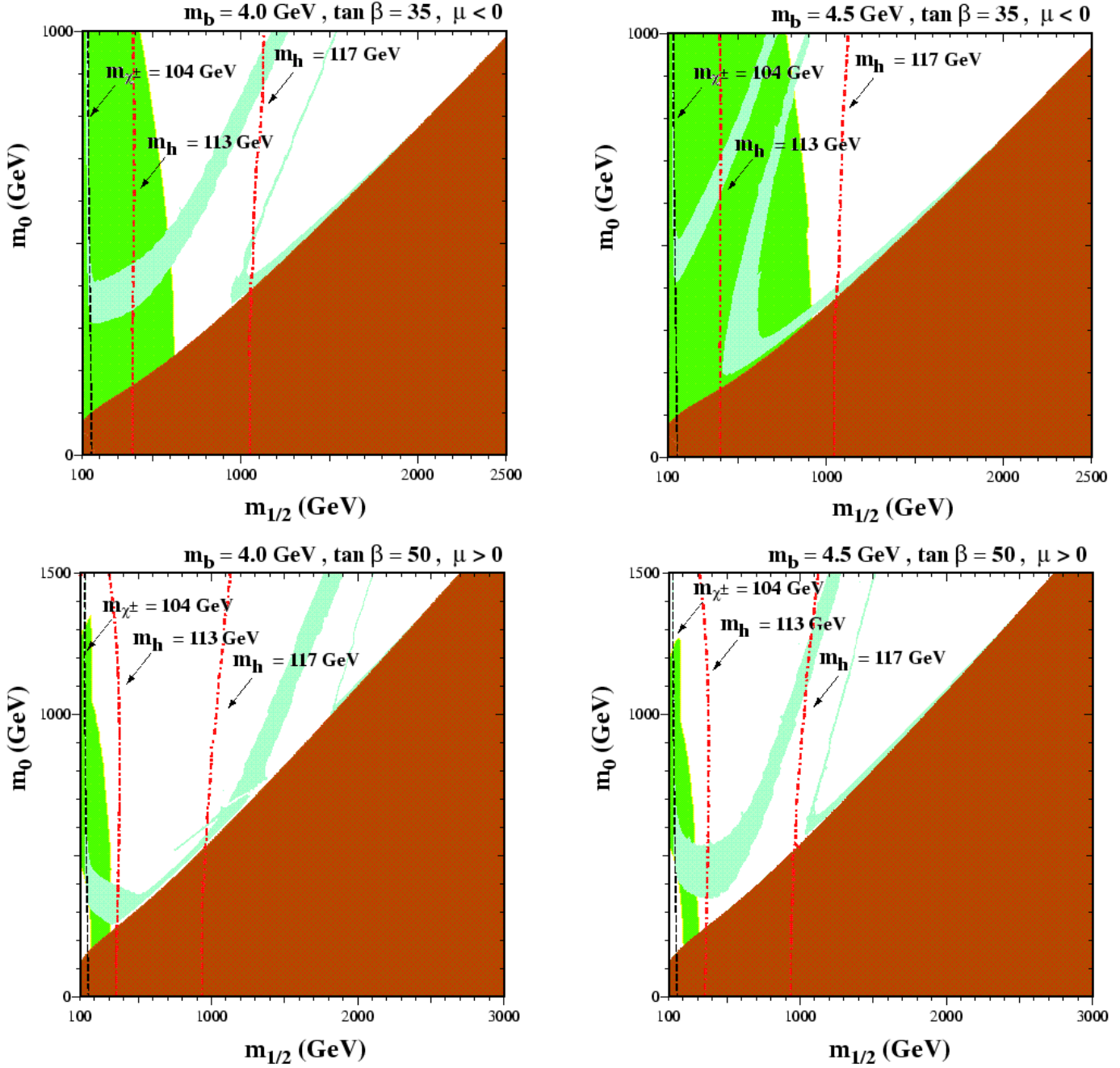


Figure 3: Comparison between the  $(m_{1/2}, m_0)$  planes for  $m_b(m_b)_{\overline{MS}} = 4.0$  and  $4.5$  GeV. Panels (a, b) are for  $\mu < 0, \tan \beta = 35$  and panels (c, d) for  $\mu > 0, \tan \beta = 50$ . In all cases, we use  $m_t = 175$  GeV and  $A_0 = 0$ . We see that the channel of low relic density due to rapid annihilation via the  $A, H$  poles appears at smaller values of  $m_{1/2}/m_0$  when  $m_b(m_b)_{\overline{MS}}$  is larger.

on  $m_{1/2}$  as seen in Fig. 1. The break and subsequent decrease in the lower limit on  $m_\chi$  at  $\tan\beta \gtrsim 30$  arise from the intersection of the rapid-annihilation region with the weakening  $b \rightarrow s\gamma$  constraint at progressively larger  $m_0$ , as also seen in Fig. 1. As previously mentioned, we find no substantial allowed regions of CMSSM parameter space above  $\tan\beta = 37.5$  for our default values of  $m_b(m_b)_{\overline{MS}}^{\overline{SM}}$ ,  $m_t$  and  $A_0$ . With these default values, we find  $m_\chi \gtrsim 140$  GeV for  $\mu > 0$ , attained in a broad minimum around  $\tan\beta \sim 25$ , and  $m_\chi \gtrsim 180$  GeV for  $\mu < 0$ , attained for  $\tan\beta \sim 15$ .

A complete discussion of the absolute lower limit on  $m_\chi$  as the auxiliary parameters  $m_b(m_b)_{\overline{MS}}^{\overline{SM}}$ ,  $m_t$  and  $A_0$  are varied over their allowed ranges lies beyond the scope of this paper, and will be presented elsewhere[30]. Here, we limit ourselves that the lower limits in Fig. 4 may be reduced significantly for different choices of these defaults. For example, if  $m_t = 180$  GeV, we find  $m_\chi \gtrsim 105$  GeV for  $\mu > 0$  and  $\tan\beta \sim 25$ , and  $m_\chi \gtrsim 145$  GeV for  $\mu < 0$  and  $\tan\beta \sim 10$  (the minimum due to the competition between the Higgs limit and the  $b \rightarrow s\gamma$  constraint occurs at lower  $\tan\beta$  than if  $m_t = 175$  GeV). Similarly, if we had chosen  $A_0 = 2m_{1/2}$ , as in the case of higher  $m_t$ , the calculated Higgs mass,  $m_h$ , would be increased and the limit on  $m_{1/2}$  (and hence  $m_\chi$ ) would be softened. In this case, we find  $m_\chi \gtrsim 95$  GeV for  $\mu > 0$  and  $\tan\beta \sim 25$  and  $m_\chi \gtrsim 140$  GeV for  $\mu < 0$  and  $\tan\beta \sim 10$ .

As also discussed in [30], these lower limits could also be relaxed somewhat if (a)  $m_h$  is below the LEP ‘signal’ at 115 GeV and closer to the LEP lower limit of 113.5 GeV, and (b) if the theoretical calculations significantly underestimate  $m_h$ , and (c) if  $\mu > 0$ , as can be seen in Fig. 2. On the other hand, if  $\mu < 0$ , the  $b \rightarrow s\gamma$  constraint is stronger than the Higgs constraint. If one believes the LEP ‘signal’, there is also an upper limit on  $m_h$ , and hence also on  $m_{1/2}$  and  $m_\chi$ . This is  $m_\chi \lesssim 400$  GeV for large  $\tan\beta$ , increasing to  $\sim 550$  GeV for  $\tan\beta = 20$  and  $\mu < 0$ .

To conclude: we have seen that an adequate treatment of the allowed CMSSM parameter space at large  $\tan\beta$  necessitates a careful analysis of coannihilations and direct-channel  $A, H$  pole annihilations. It is also essential to treat carefully the value and the renormalization of  $m_b$ . The most recent LEP lower limit on  $m_h$  and recent improvements in the experimental value and the theoretical treatment of  $b \rightarrow s\gamma$  decay at large  $\tan\beta$  also play important roles. At large  $\tan\beta$ , the CMSSM survives these and the supersymmetric dark matter constraint for  $\mu < 0$  only thanks to the extensions of parameter space made by coannihilations and direct-channel  $A, H$  pole annihilations. These also play important roles for  $\mu > 0$ . Putting together all the available constraints, we find that  $m_\chi \gtrsim 140(180)$  GeV for  $\mu > 0(\mu < 0)$  and our default choices of  $m_b(m_b)_{\overline{MS}}^{\overline{SM}}$ ,  $m_t$  and  $A_0$ . More complete discussions of the roles of  $m_t$  and  $A_0$  in the CMSSM, and a treatment of the more general MSSM without universality

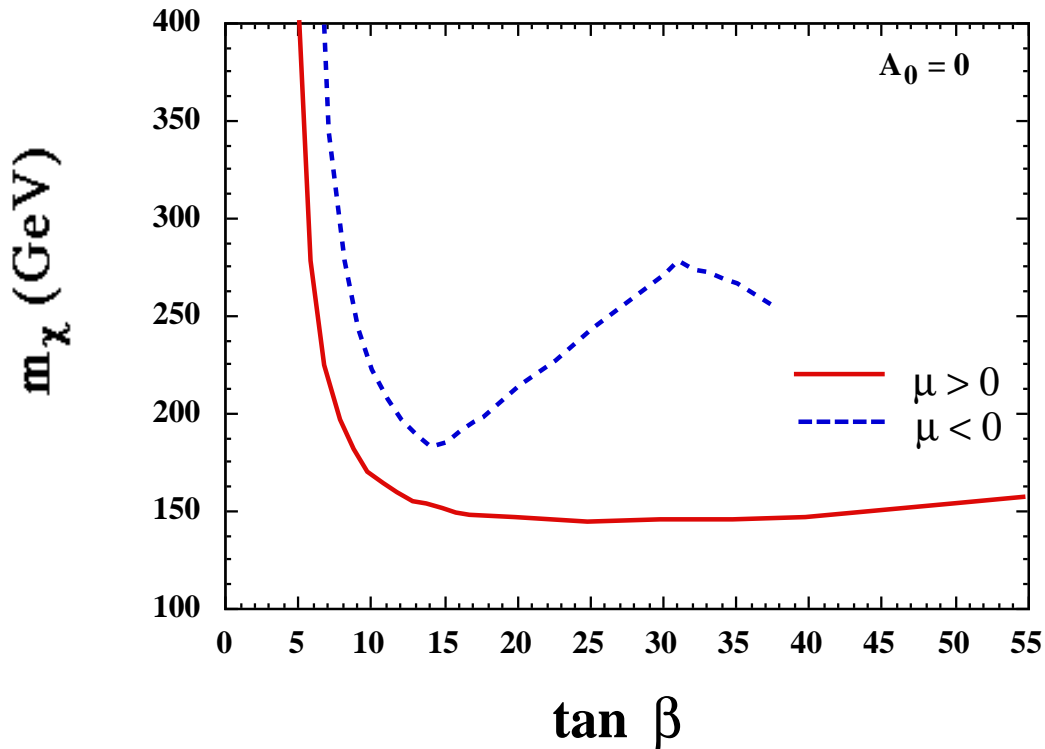


Figure 4: Lower limits on the LSP mass  $m_\chi$  obtained as functions of  $\tan \beta$  for both signs of  $\mu$ . We use as defaults  $m_b(m_b)_{\overline{MS}} = 4.25$ ,  $m_t = 175$  GeV and  $A_0 = 0$ .

assumptions, are left to a future paper [30].

### Acknowledgments

We would like to thank W. de Boer and P. Gambino for useful discussions. The work of K.A.O. was partially supported by DOE grant DE-FG02-94ER-40823, and that of M.S. by NSF grant PHY-97-22022.

### References

- [1] For a recent compilation of LEP search data, as presented on Sept. 5th, 2000, see: T. Junk, hep-ex/0101015.
- [2] ALEPH collaboration, R. Barate *et al.*, Phys. Lett. **B495** (2000) 1 [hep-ex/0011045]; L3 collaboration, M. Acciarri *et al.*, Phys. Lett. **B495** (2000) 18 [hep-ex/0011043];

- OPAL collaboration, G. Abbiendi *et al.*, hep-ex/0101014;  
 DELPHI collaboration, P. Abreu *et al.*, preprint 0285,  
<http://delphiwww.cern.ch/~pubxx/www/delsec/papers/public/papers.html>.  
 For a compilation of the LEP data presented on Nov. 3rd, 2000, see:  
 P. Igo-Kemenes, for the LEP Higgs working group,  
<http://lephiggs.web.cern.ch/LEPHIGGS/talks/index.html>.
- [3] CLEO Collaboration, M.S. Alam *et al.*, Phys. Rev. Lett. **74** (1995) 2885 as updated in S. Ahmed *et al.*, CLEO CONF 99-10; BELLE Collaboration, BELLE-CONF-0003, contribution to the 30th International conference on High-Energy Physics, Osaka, 2000.
- [4] J. Ellis, J.S. Hagelin, D.V. Nanopoulos, K.A. Olive and M. Srednicki, Nucl. Phys. **B238** (1984) 453; see also H. Goldberg, Phys. Rev. Lett. **50** (1983) 1419.
- [5] J. Ellis, T. Falk, K. A. Olive and M. Schmitt, Phys. Lett. **B388** (1996) 97 and Phys. Lett. **B413** (1997) 355; J. Ellis, T. Falk, G. Ganis, K. A. Olive and M. Schmitt, Phys. Rev. **D58** (1998) 095002.
- [6] J. Ellis, T. Falk and K. A. Olive, Phys. Lett. **B444**, 367 (1998); J. Ellis, T. Falk, K. A. Olive and M. Srednicki, Astropart. Phys. **13** (2000) 181.
- [7] J. Ellis, T. Falk, G. Ganis and K. A. Olive, Phys. Rev. **D62** (2000) 075010.
- [8] J. Ellis, G. Ganis, D. V. Nanopoulos and K. A. Olive, hep-ph/0009355.
- [9] A. Bottino, V. de Alfaro, N. Fornengo, G. Mignola and S. Scopel, Astropart. Phys. **1**, 61 (1992); P. Nath and R. Arnowitt, Phys. Rev. Lett. **70**, 3696 (1993); G. L. Kane, C. Kolda, L. Roszkowski and J. D. Wells, Phys. Rev. **D49**, 6173 (1994); R. Arnowitt and P. Nath, Phys. Rev. **D54**, 2374 (1996).
- [10] M. Drees and M. M. Nojiri, Phys. Rev. **D47**, 376 (1993);
- [11] H. Baer and M. Brhlik, Phys. Rev. **D53** (1996) 597 and Phys. Rev. **D57** (1998) 567; H. Baer, M. Brhlik, M. A. Diaz, J. Ferrandis, P. Mercadante, P. Quintana and X. Tata, Phys. Rev. **D63** (2001) 015007.
- [12] J. Edsjo and P. Gondolo, Phys. Rev. **D56** (1997) 1879.
- [13] V. Barger and C. Kao, Phys. Rev. **D57** (1998) 3131.

- [14] M. E. Gómez, G. Lazarides and C. Pallis, Phys. Rev. **D61**, 123512 (2000) and Phys. Lett. **B487**, 313 (2000).
- [15] For another recent analysis taking account of coannihilation effects, see:  
A. B. Lahanas, D. V. Nanopoulos and V. C. Spanos, Phys. Rev. **D62** (2000) 023515.
- [16] For recent reviews, see: M. Drees, hep-ph/0101217; R. Arnowitt, B. Dutta and Y. Santoso, hep-ph/0101020; A. Corsetti and P. Nath, hep-ph/0011313; A. Bottino, N. Fornengo and S. Scopel, hep-ph/0012377; L. Bergstrom, Rept. Prog. Phys. **63** (2000) 793; G. Ganis, hep-ex/0102013.
- [17] M. Ciuchini, G. Degrassi, P. Gambino, G.F. Giudice, Nucl.Phys. **B527** (1998) 21; P. Ciafaloni, A. Romanino, A. Strumia, Nucl.Phys.**B524** (1998) 361; F. Borzumati and C. Greub, Phys. Rev. **D58** (1998) 074004; M. Ciuchini, G. Degrassi, P. Gambino and G.F. Giudice, Nucl. Phys. **B534** (1998) 3.
- [18] C. Degrassi, P. Gambino and G. F. Giudice, JHEP **0012** (2000) 009; see also M. Carena, D. Garcia, U. Nierste and C. E. Wagner, hep-ph/0010003.
- [19] K. Griest and D. Seckel, Phys. Rev. **D43** (1991) 3191; P. Gondolo and G. Gelmini, Nucl. Phys. **B360** (1991) 145.
- [20] A. B. Lahanas, D. V. Nanopoulos and V. C. Spanos, hep-ph/0009065.
- [21] S. Mizuta and M. Yamaguchi, Phys. Lett. **B298** (1993) 120.
- [22] C. Boehm, A. Djouadi and M. Drees, Phys. Rev. **D62** (2000) 035012.
- [23] P. Gondolo, J. Edsjo, L. Bergstrom, P. Ullio and E. A. Baltz, astro-ph/0012234.
- [24] B. Abbott *et al.*, D0 Collaboration, Phys. Rev. **D60** (1999) 031101; A. Nomerotski, for the CDF Collaboration, *Talk given at the 34th Rencontres De Moriond: Electroweak Interactions and Unified Theories, Les Arcs, France, 13-20 Mar 1999*, Fermilab CONF-99-117-E.
- [25] J. Ellis, M.K. Gaillard and D.V. Nanopoulos, Nucl. Phys. **B106** (1976) 292; B.L. Ioffe and V.A. Khoze, Sov. J. Part. Nucl. **9** (1978) 50; B.W. Lee, C. Quigg and H.B. Thacker, Phys. Rev. **D16** (1977) 1519.

- [26] For our numerical analysis, we use the results of: H.E. Haber, R. Hempfling and A.H. Hoang, *Zeit. für Phys.* **C75** (1997) 539; see also M. Carena, M. Quiros and C.E.M. Wagner, *Nucl. Phys.* **B461** (1996) 407. We have checked that these results agree, within the expected uncertainties, with those of M. Carena, H. E. Haber, S. Heinemeyer, W. Hollik, C. E. Wagner and G. Weiglein, *Nucl. Phys.* **B580** (2000) 29. For other precise MSSM Higgs mass calculations, see J. R. Espinosa and R. Zhang, *JHEP* **0003** (2000) 026 and *Nucl. Phys. B* **586** (2000) 3.
- [27] A. Katsikatsou, A. B. Lahanas, D. V. Nanopoulos and V. C. Spanos, hep-ph/0011370.
- [28] M. Carena, J. Ellis, A. Pilaftsis and C. E. Wagner, *Phys. Lett.* **B495** (2000) 155.
- [29] M. Spira, *Fortsch. Phys.* **46**, 203 (1998), hep-ph/9705337.
- [30] J. Ellis, T. Falk, G. Ganis, K. A. Olive and M. Srednicki, to appear.
- [31] G. Martinelli and C. T. Sachrajda, *Nucl. Phys.* **B559** (1999) 429, as updated by C. T. Sachrajda, hep-lat/0101003.
- [32] D.E. Groom *et al.*, *Euro. Phys. J.* **C15** (2000) 1, <http://pdg.lbl.gov/>.
- [33] M. Beneke and A. Signer, *Phys. Lett.* **B471** (1999) 233; A. H. Hoang, *Phys. Rev.* **D61** (2000) 034005 and hep-ph/0008102.
- [34] K. G. Chetyrkin, *Phys. Lett.* **B404** (1997) 161; for a recent review, see: F. A. Chishtie and V. Elias, hep-ph/0012254.
- [35] B. C. Allanach and S. F. King, *Nucl. Phys.* **B507** (1997) 91.
- [36] D. M. Pierce, J. A. Bagger, K. Matchev and R. Zhang, *Nucl. Phys.* **B491**, 3 (1997).
- [37] S. P. Martin and M. T. Vaughn, *Phys. Rev.* **D50**, 2282 (1994).
- [38] J. L. Feng, K. T. Matchev and F. Wilczek, *Phys. Lett.* **B482** (2000) 388, and *Phys. Rev.* **D63** (2001) 045024.